Supporting Information

Intercalation of Cobalt into the Interlayer of Birnessite Improves Oxygen Evolution Catalysis

*Akila C. Thenuwara[1,3], Samantha L. Shumlas[1,3], Nuwan H. Attanayake[1,3], Yaroslav V. Aulin[1,3], Ian G. McKendry[1,3], Qiao Qiao [2,3], Yimei Zhu[2,3], Eric Borguet[1,3], Michael J. Zdilla[1,3] and Daniel R. Strongin[1,3] **

[1]Department of Chemistry, Temple University, Beury Hall, 1901 N. 13th St, Philadelphia, Pennsylvania, 19122, United States

[2]Department of Condensed Matter Physics and Materials Science, Brookhaven National Laboratory, Upton, New York 11973, United States

[3]Center for Computational Design of Functional Layered Materials (CCDM), Temple University, Philadelphia, Pennsylvania, 19122, United States

*dstrongi@temple.edu

Table of Content **Page**

List of Figures & Tables

Experimental

Materials and Methods

All the chemicals used here were purchased from commercial vendors and used without any further purification. X-ray diffraction (XRD) data were acquired on a Bruker Kappa APEX II DUO diffractometer using Mo Kα radiation from a sealed molybdenum tube with a TRIUMPH monochromator. X-ray photoelectron spectroscopy (XPS) was conducted with a Thermo Scientific K-alpha+ at the University of Delaware. A JEOL JEM-1400 microscope operating at 120 kV was used to obtain transmission electron microscopy (TEM) images. SAED patterns, STEM images and EEL spectra were taken using an aberration corrected JEOL JEM-ARM200CF scanning transmission electron microscope operated at 200 kV. Atomic resolution STEM images were taken with an annular bright-field detector. The image contrast was inverted so that the atoms appear to be bright, and the inverted ABF images were processed with a low-pass filter to remove high frequency noise. The STEM image for the EELS line scan was taken with an annular dark-field detector. Scanning electron microscopy (SEM) images were obtained using a FEI Quanta 450 FEG-SEM microscope operating at 30 kV. Energy dispersive spectroscopy (EDS) analysis was performed with an Oxford systems nano-analysis EDS system, using Aztec 2.1 as the analyzing software. Elemental analysis was performed using a Thermo Scientific iCAP 7000 Series Inductively Coupled Plasma with an Optical Emission Spectrometer

(ICP-OES). Raman measurements were performed using a Horiba Labram HR800 Evolution confocal Raman spectrometer with 532 nm excitation and a 100X objective. All samples were pressed into pellets by applying pressure to obtain a smooth surface for Raman analysis. The Brunauer-Emmett-Teller (BET) specific surface area measurements were performed by single-point BET N_2 adsorption using an ASAP 2020 surface area analyzer (Micromeritics).

Synthesis of potassium birnessite. Hydrochloric acid (4 M, 50.0 mL) was added drop wise via a syringe pump at 1 mL/min to a heated and stirred (80 ˚C, 360 rpm) solution of potassium permanganate ($KMnO_4$, 0.200 M, 250 mL) in a 400 mL beaker. Heating continued at 80 ˚C for an additional 0.5 h after addition was completed. The resulting 300 mL solution was then covered to prevent excessive evaporation overnight and aged for 15 h at 50 ˚C. Finally, the resulting suspension was washed several times with distilled water and dried at room temperature.

α-cobalt hydroxide synthesis. A colorless solution was formed by dissolving cobalt chloride hexahydrate ($CoCl_2 \bullet 6H_2O$) and NH_4F in distilled water ($[Co^{2+}]$ = 0.6 mol dm^{-3}) while keeping the molar ratio of NH_4F to Co^{2+} equal to 0.25. Propylene oxide was used as the precipitation agent and the molar ratio of propylene oxide and metal ions were kept at 10. A precipitate formed within 0.5–2 h under vigorous stirring. After reaction for 24 h, green colored cobalt hydroxide nanosheets were obtained by vacuum filtration, water-washed, and dried at 80°C.

β-cobalt hydroxide synthesis. β-$Co(OH)_2$ nanostructures were synthesized by a hydrothermal synthesis method. First, $CoCl_2 \bullet 6H_2O$ (2 mmol) was dissolved in 40 mL of distilled water and 1.0

mL of $N(CH_2CH_3)_3$ was added to the Co-containing solution while being constantly stirred. Next, the resultant slurry was transferred to a 50 mL autoclave and heated at 180 °C for 24 h in a furnace. The autoclave was then left to cool to room temperature. Finally, the solid product was recovered, washed with water several times, and air-dried.

Co_3O_4 synthesis. Cobalt oxide was formed by dissolving $CoCl_2 \bullet 6H_2O$ and NH_4F, in distilled water ($[Co^{2+}]$ = 0.6 mol dm^{-3}) while keeping the molar ratio of NH_4F to Co^{2+} equal to 2. Propylene oxide was used as the precipitation agent and the molar ratio of propylene oxide to metal ions was kept at 10. A precipitate was then produced within 0.5–2 h under vigorous stirring. After reaction for 24 h, the resulting pink precipitate was obtained by vacuum filtration. The precipitate was then water-washed and air-dried. Co_3O_4 was produced by annealing the pink powder in air at 400 ˚C for 4 h.

Synthesis of cobalt substituted birnessite. Hydrochloric acid (2 M, 50.0 mL) and cobalt(II) chloride hexahydrate (47 mmol, 50.0 mL) were added simultaneously via a syringe pump operating at 1 mL/min to a heated and stirred solution (80^{o}C, 360 rpm) of $KMnO_4$ (0.200 M, 250 mL). After the addition was completed, heating at 80^{o}C was continued for 30 min at which point the temperature was reduced to 40^o C and material was aged overnight. The resulting blue-black precipitate was then washed several times with distilled water via centrifugation and dried in air at room temperature.

Synthesis of birnessite intercalated with cobalt. Co-intercalated birnessite (referred to as Co^{2+}/birnessite hereafter) was prepared via a wet chemical ion exchange reaction. The cobalt

precursor solution was prepared by adding 0.100 g (0.422 mmol) of $CoCl_2 \bullet 6H_2O$ to 20 mL of deionized water (18.3 MΩ cm). A stoichiometric amount (19 µL, 0.204 mmol) of hydrazine solution (35 wt. % in H_2O) was added to the cobalt precursor solution. A noticeable color change from pink to pale green was observed after the addition of hydrazine, which is an indication of the formation of the cobalt-hydrazine complex (Equation S1). After stirring for 5 min, 0.100 g of synthetic birnessite was added to the green colored cobalt-hydrazine complex containing solution and the suspension was stirred vigorously for 30 min. Finally, the solution was vacuum filtered and the residue washed with deionized water. In order to examine the effect of reaction time, a series of Co^{2+}/birnessite samples were synthesized by changing the exposure time of birnessite to the cobalt-hydrazine complex from 30 to 60 min.

$$CoCl_{2\,(s)} + xN_2H_{4\,(aq)} + yH_2O_{\,(aq)} \longrightarrow [Co(N_2H_4)_x(H_2O)_y]^{2+}{}_{(aq)} + 2Cl^-_{(aq)} \qquad \text{(S1)}$$

Electron microscopy Characterization

TEM selected area electron diffraction (SAED) patterns were taken from both pristine and Co^{2+}/birnessite, as shown in Figure S16. Comparing to the SAED pattern from Co^{2+}/birnessite, the one from pristine birnessite show more and sharper diffraction rings, suggesting better crystallinity, in accordance with the XRD results. Atomic resolution STEM images further confirm the crystal quality down to atomic level. Figure S2 (a) shows the atomic structure of the pristine birnessite from its [010] direction that matches the atomic model given in Figure S2 (b), while a lower magnification image of the layered structure is shown in Figure S2 (c). Despite slight bending, the pristine birnessite manifests good crystallinity with virtually no defects. As opposed to pristine birnessite, Co^{2+}/birnessite is found to be defect-rich. As shown in Figures S3 (a-c), edge dislocations and grain boundaries are clearly visible from the cross sectional images.

Electrochemical Characterization

The electrocatalytic studies were conducted in 1 M KOH (pH ~14) or 0.5 M phosphate buffer (pH~7) using a CHI 660E potentiostat operating in a standard three-electrode configuration at ambient temperature (22 ± 2 °C). Glassy carbon (GC) electrodes (3 mm diameter from CH instruments) were used as working electrodes. Before electrochemical experiments the GC electrodes were polished using 1, 0.3, and 0.05 μm alumina powder, respectively, and sonicated in DI water to clean the electrode surfaces. All the potentials were measured with respect to a calomel reference electrode (CH instruments) and Pt wire was used as the counter electrode. The working electrode was prepared by drop casting 5 μL of catalyst ink suspension on the glassy carbon electrode (loading 0.28 mg/cm^2). Ink solutions were prepared as follows: 4 mg of catalyst and 4 mg of carbon (VulcanXC-72) were added to 1 mL isopropanol and 35 μL of Nafion solution (5% in alcohol, Ion Power Inc.) and the resulting mixture was sonicated for at least 30 min to form the catalyst ink. All polarization curves were recorded at a scan rate of 10 mV/s. For all the catalysts tested, polarization curves were replicated at least 5 times. The overpotential (at a current density of 10 mA/cm^2) and Tafel slopes reported are based on an analysis of these data. Estimation of the electrochemically active surface area (ECSA) of the catalysts was carried out by plotting charging current density differences ($\Delta j = ja - jc$) as a function of scan rate. The charging current density differences can be obtained by performing cyclic voltammetry (CV) at different scan rates in a potential window of 100 mV, where the

open circuit potential (OCP) falls in the middle. The double layer capacitance was estimated from the slope of the charging current density differences at OCP vs scan rate plot. The slope is twice the double layer capacitance. Since double layer capacitance is proportional to the ECSA of the catalyst, the ratio of double layer capacitance can be considered as the ratio of ECSA. For stability testing, carbon fiber paper (CFP) was also used as electrodes. For the CFP electrodes, the catalyst loading was 1 mg/cm^2. For Faradaic efficiency determination an H-type cell was used. Electrolysis was performed at a constant current of 7 mA and the electrochemically-generated headspace gas was analyzed using a gas chromatograph (HP 5890 series II) equipped with a molecular sieve column and thermal conductivity detector.

Catalytic parameter calculations

The turnover frequency (TOF) value is calculated from the equation:

$$TOF = \frac{JA}{4Fn}$$

Where, J is the measured current density (mA cm^{-2}) at η = 0.40 V, A is the geometric area of the electrode, n is the number of moles of catalyst, and F is the Faraday constant (96500 C mol^{-1}).

The mass activity was calculated from following equation:

$$mass\ activity = \frac{J}{m}$$

The mass activity (A g^{-1}) was calculated on the basis of the catalyst loading m = 0.28 mg cm^{-2} and the measured current density j (mA cm^{-2}) at η = 0.40 V.

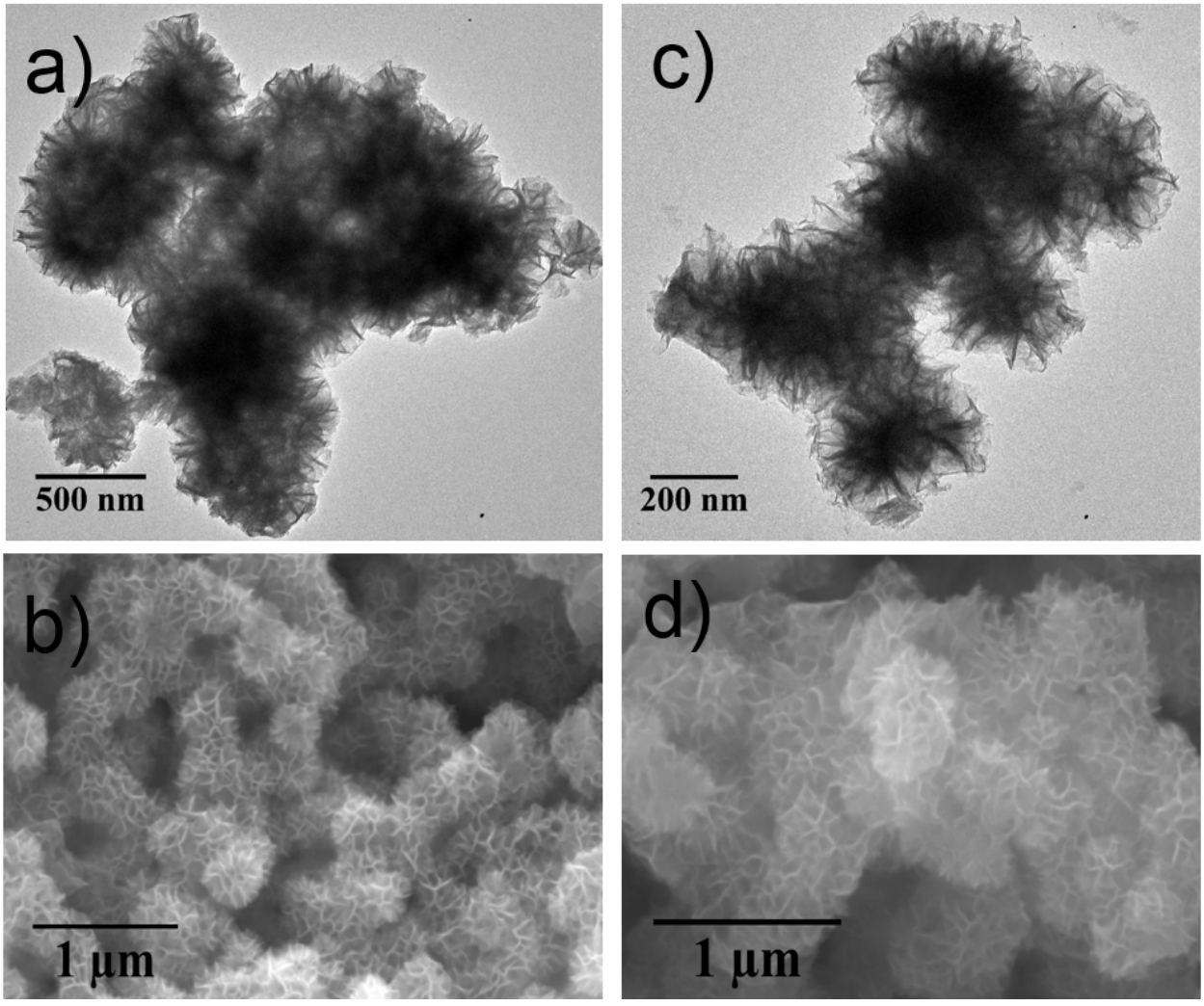

Figure S1. Electron micrographs of Co^{2+}/ birnessite: (a) TEM and (b) SEM. Micrographs of birnessite: (c) TEM and (d) SEM. Co-intercalation did not significantly alter the morphology of birnessite.

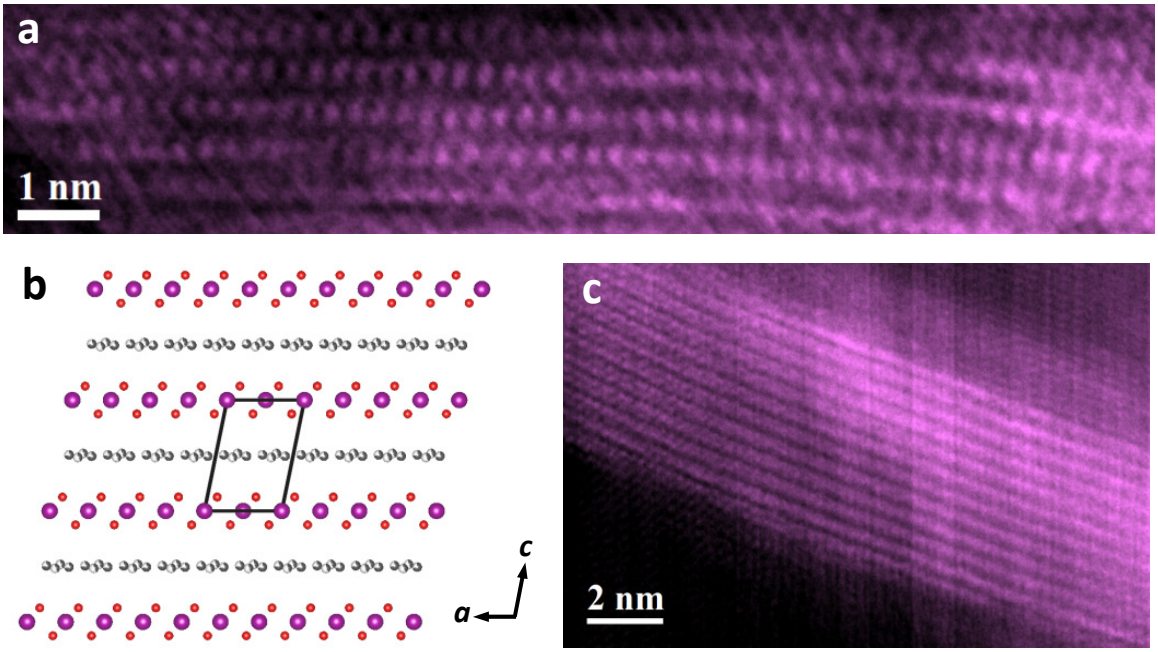

Figure S2. Inverted ABF image of pristine birnessite. (a) atomic resolution image of pristine birnessite, view from [010] direction; (b) atomic model of birnessite from its [010] direction, the black parallelogram indicates the primitive unit cell; (c) lower magnification image showing layered structure with good crystallinity, virtually with no defects.

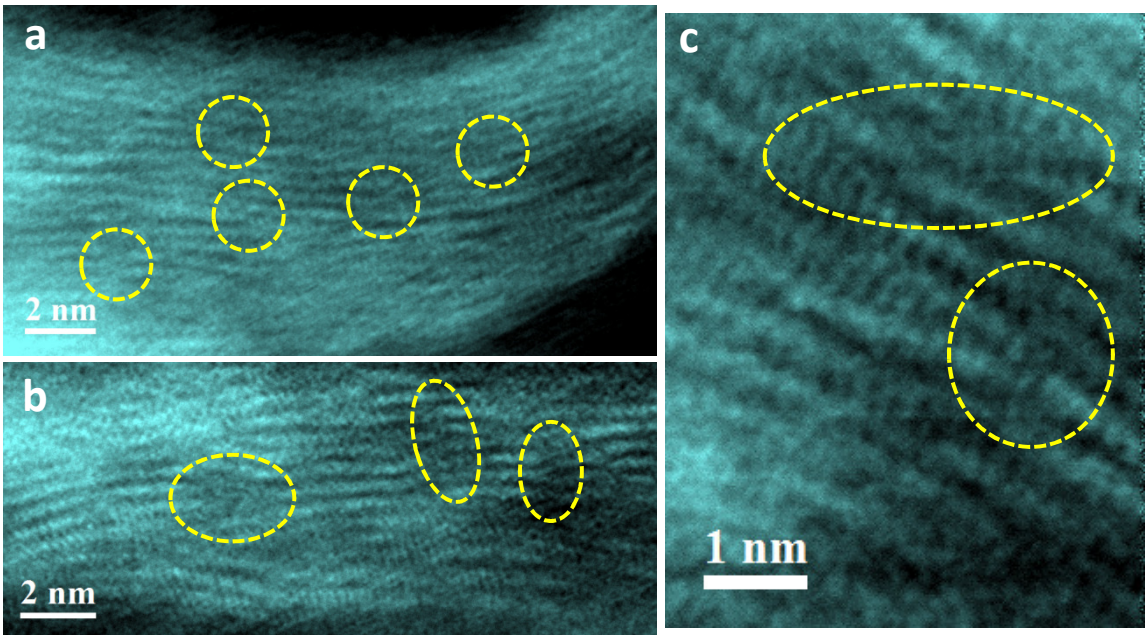

Figure S3. Inverted ABF image of Co^{2+}/birnessite. (a-c) High resolution images of the cross section of Co^{2+}/birnessite, yellow circles indicate defects such as edge dislocations and grain boundaries.

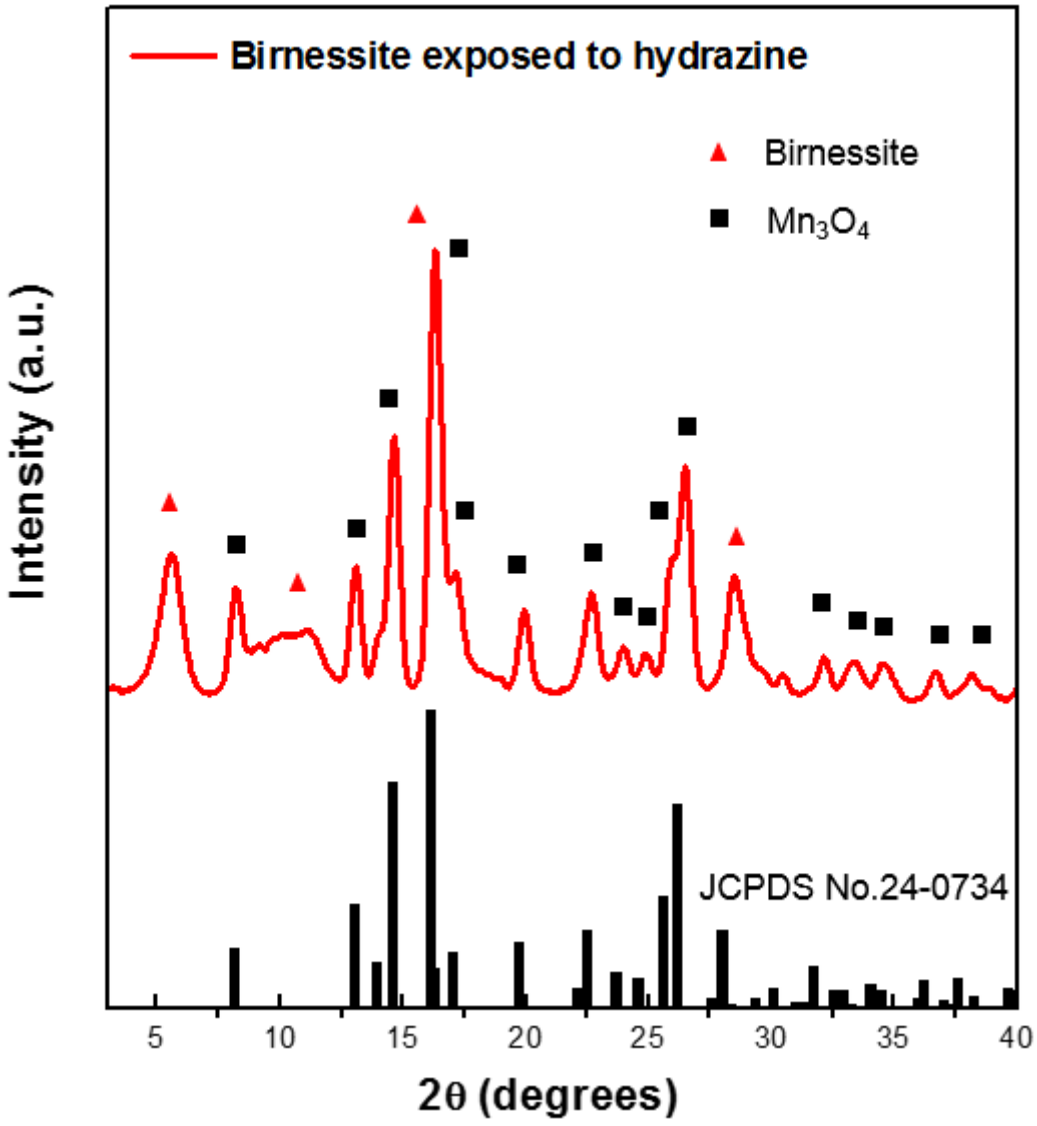
Birnessite exposed to hydrazine
Birnessite
Mn_3O_4
JCPDS No.24-0734
Intensity (a.u.)
5
10
15
20
25
30
35
40
2θ (degrees)

Figure S4. Experimental XRD pattern for birnessite exposed to hydrazine (without Co^{2+} ions) shown together with the diffraction peak positions associated with tetragonal Mn_3O_4 (JCPDS no. 24-0734). A comparison suggests that birnessite transforms into Mn_3O_4 when exposed to hydrazine.

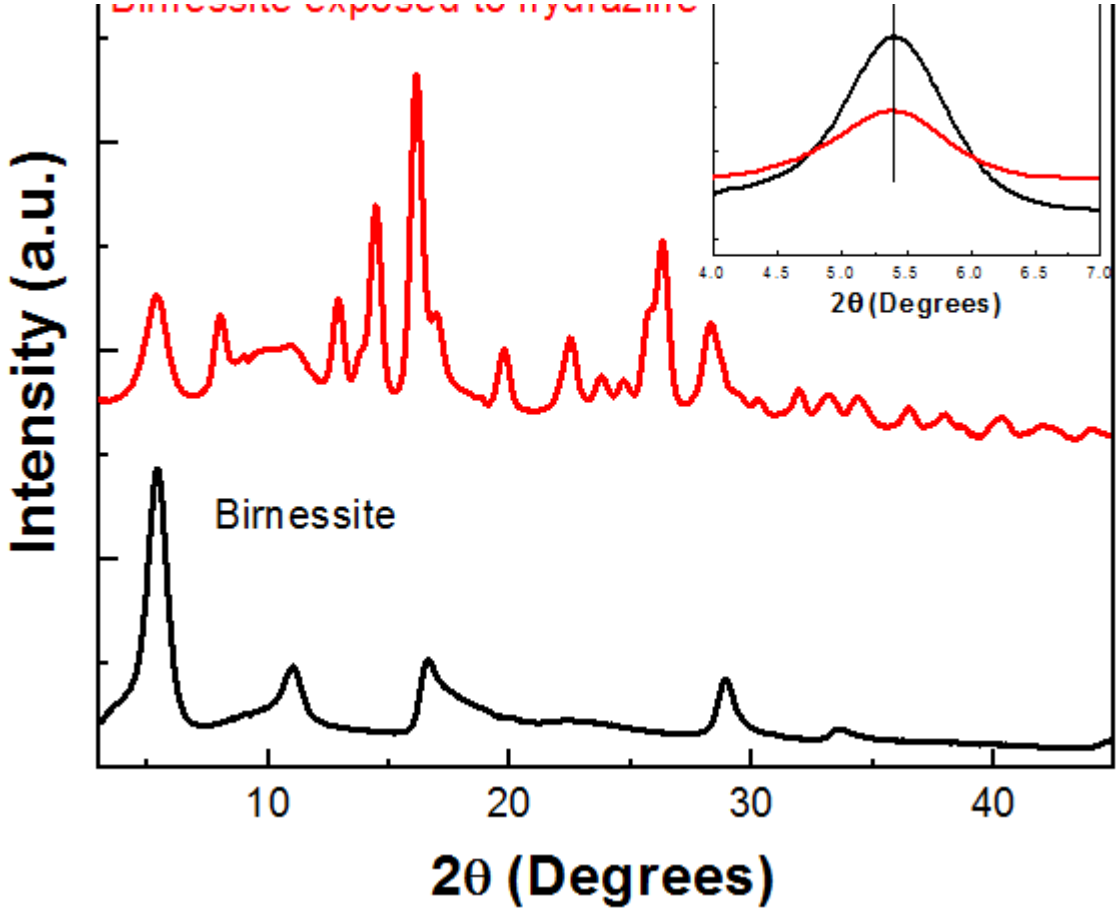

Figure S5. XRD spectra of birnessite and birnessite exposed to hydrazine. Inset is the enlarged (001) region that corresponds to the interlayer spacing. The spectra suggest that hydrazine does not alter interlayer spacing of birnessite (i.e., octahedral sheet) does not alter the interlayer spacing.

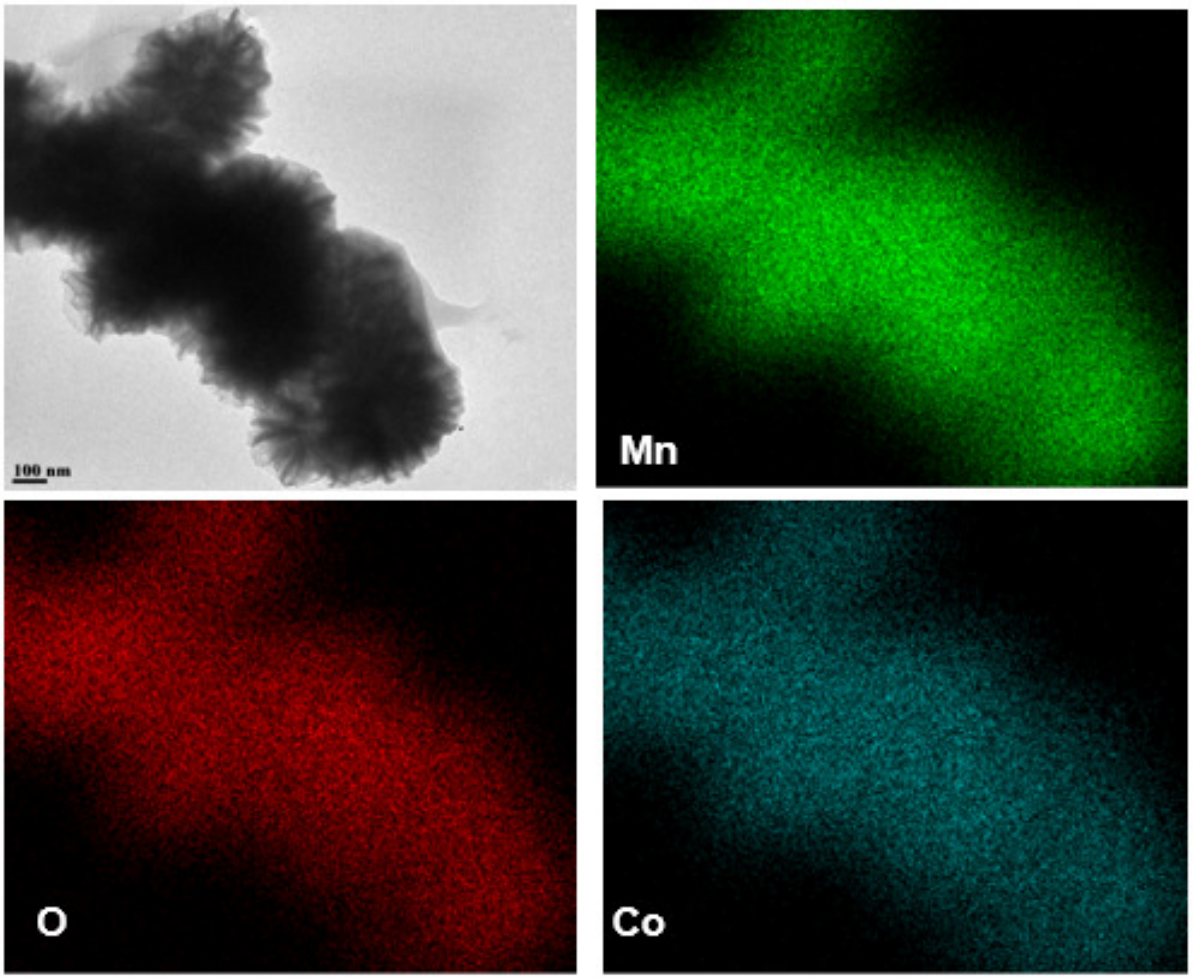

Figure S6. Top left panel is a STEM micrograph for Co^{2+}/ Birnessite. Also included in the figure are energy dispersive spectroscopy (EDS) elemental maps for Mn, O and Co.

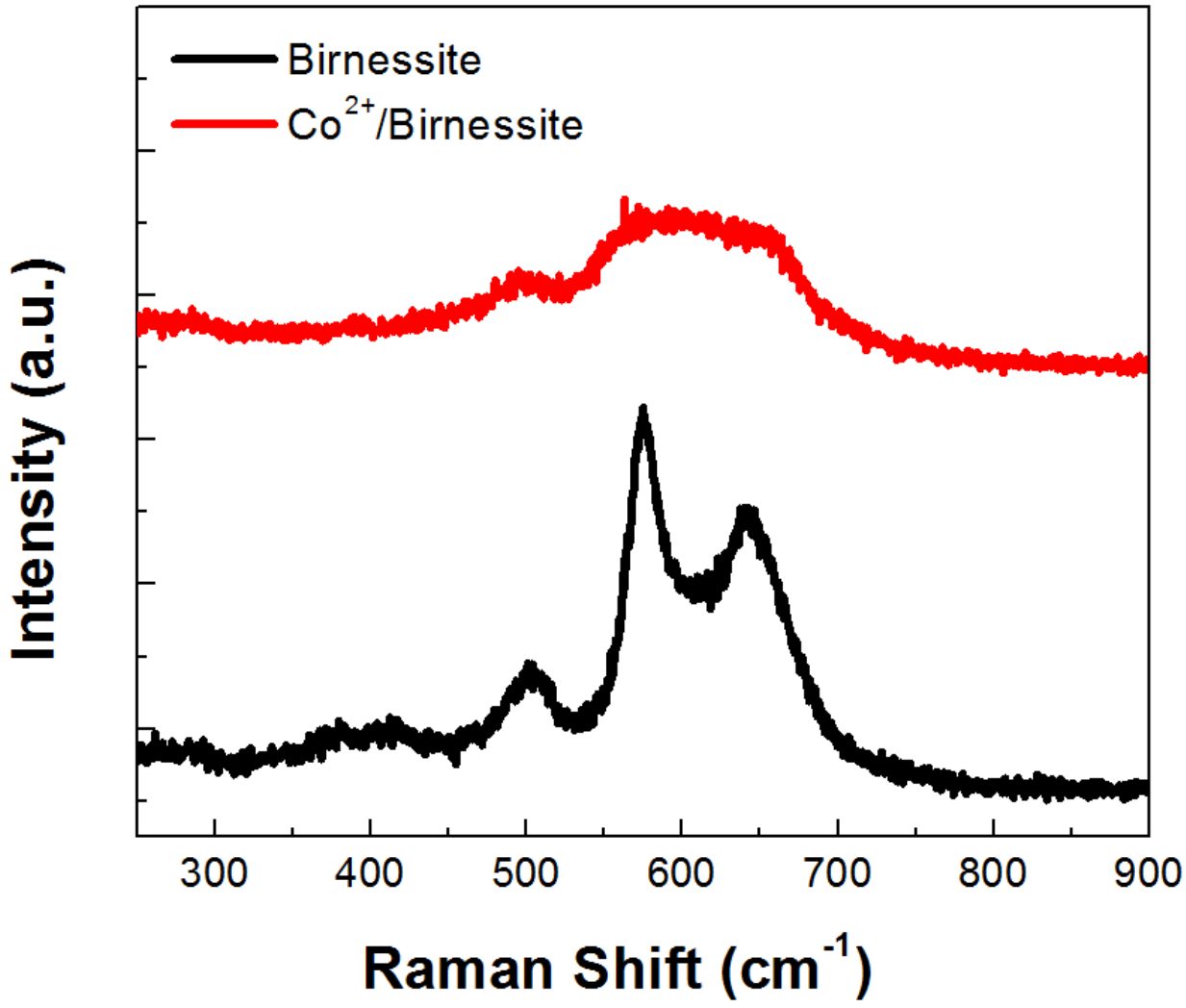

Figure S7. Raman spectra of birnessite and Co^{2+}/birnessite. We attribute the broadening of the Raman peaks to the disorder in the birnessite lattice induced by the presence of cobalt in the interlayer region.

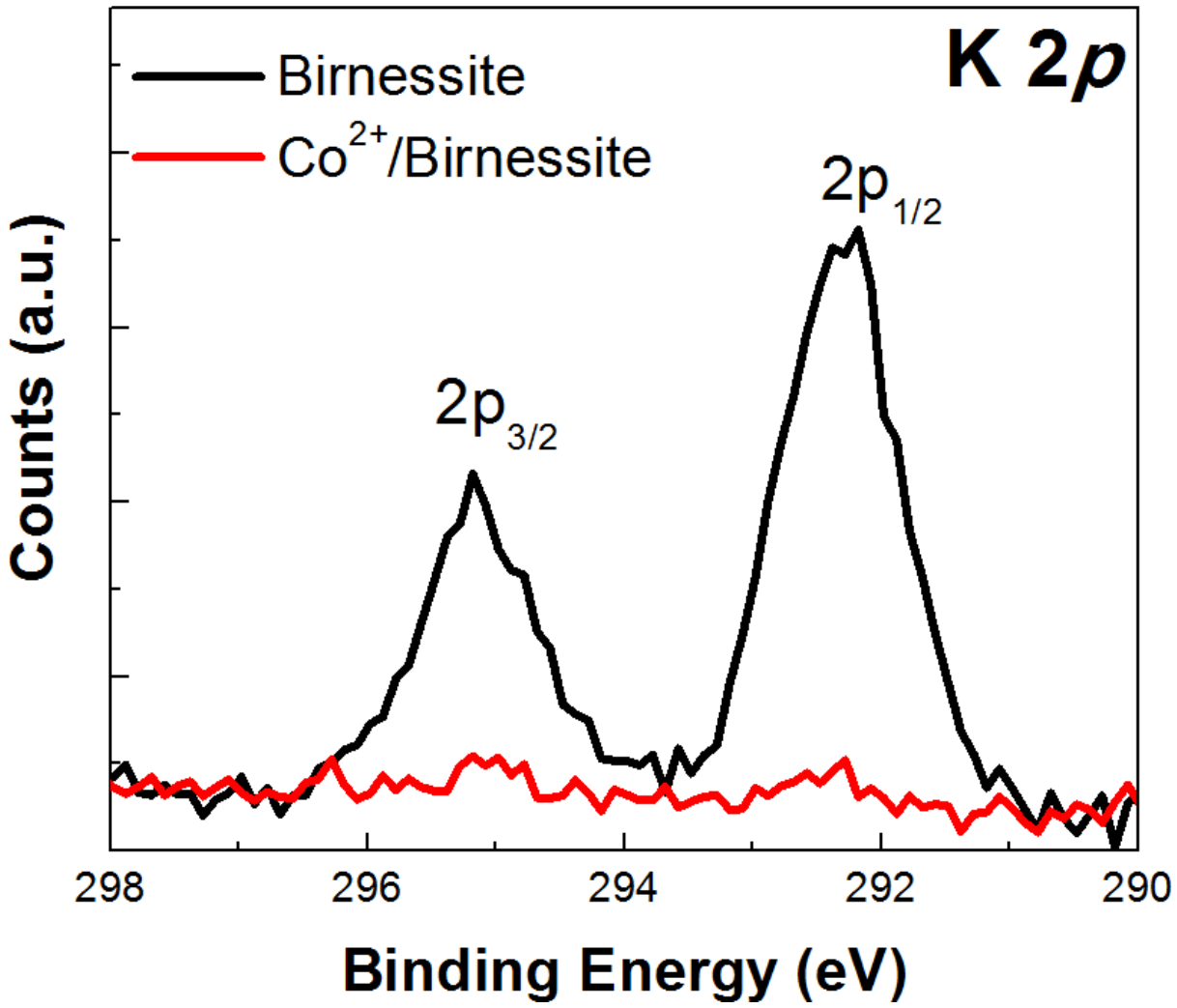

Figure S8. K 2*p* XPS of birnessite and Co^{2+}/birnessite. An evaluation of the spectra shows the loss of potassium ions from the birnessite interlayer as a consequence of the intercalation reaction.

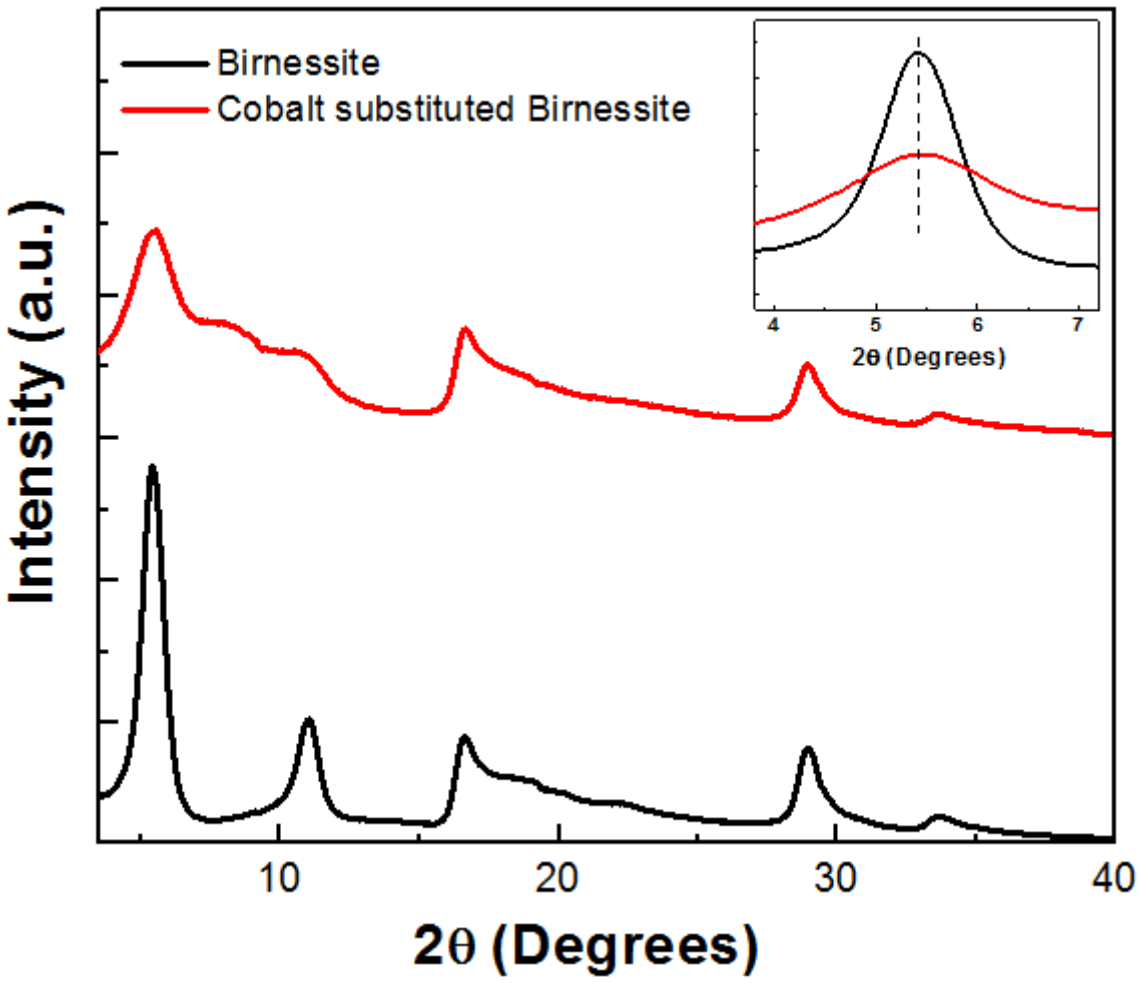

Figure S9. XRD diffractograms of birnessite and Co substituted birnessite. Inset is the enlarged (001) region that corresponds to the interlayer spacing. The spectra suggest that substitution of cobalt into the birnessite structure (i.e., octahedral sheet) does not alter the interlayer spacing.

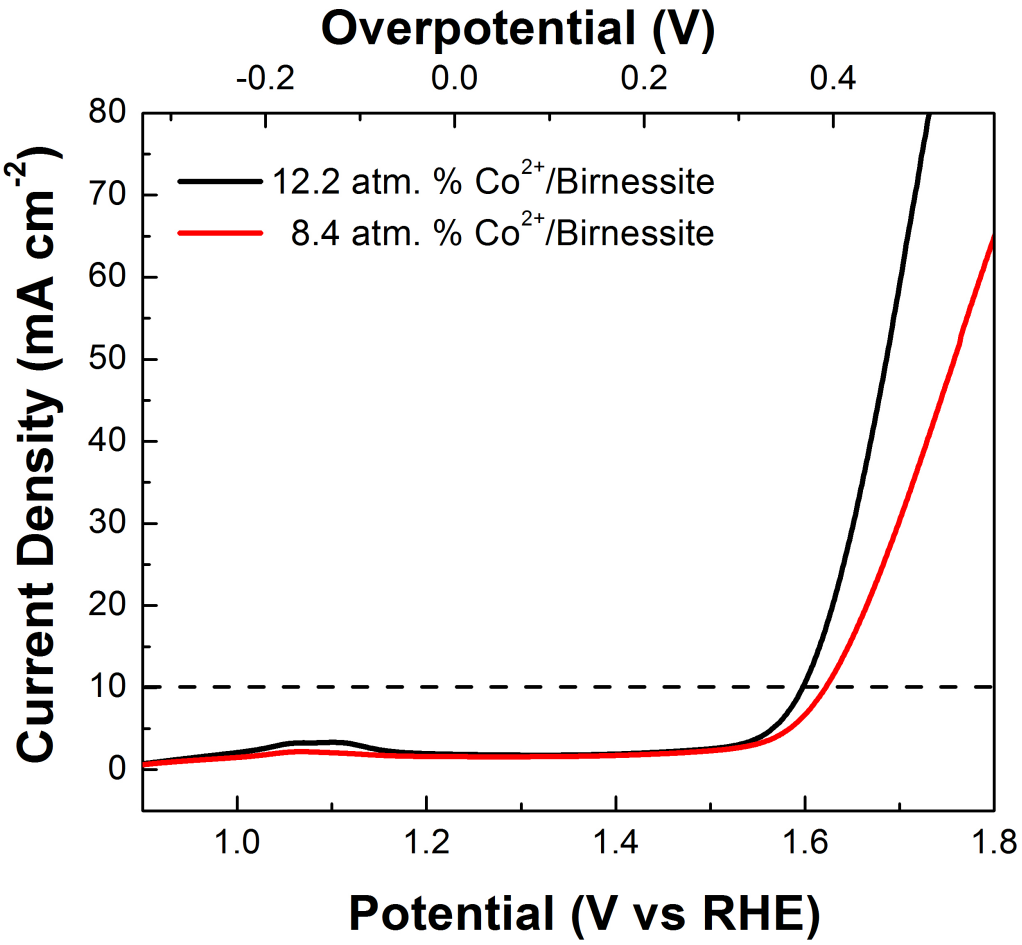

Figure S10. Polarizations curves for 12.2 atm. % Co^{2+}/birnessite and 8.4 atm. % Co^{2+}/birnessite in 1 M KOH.

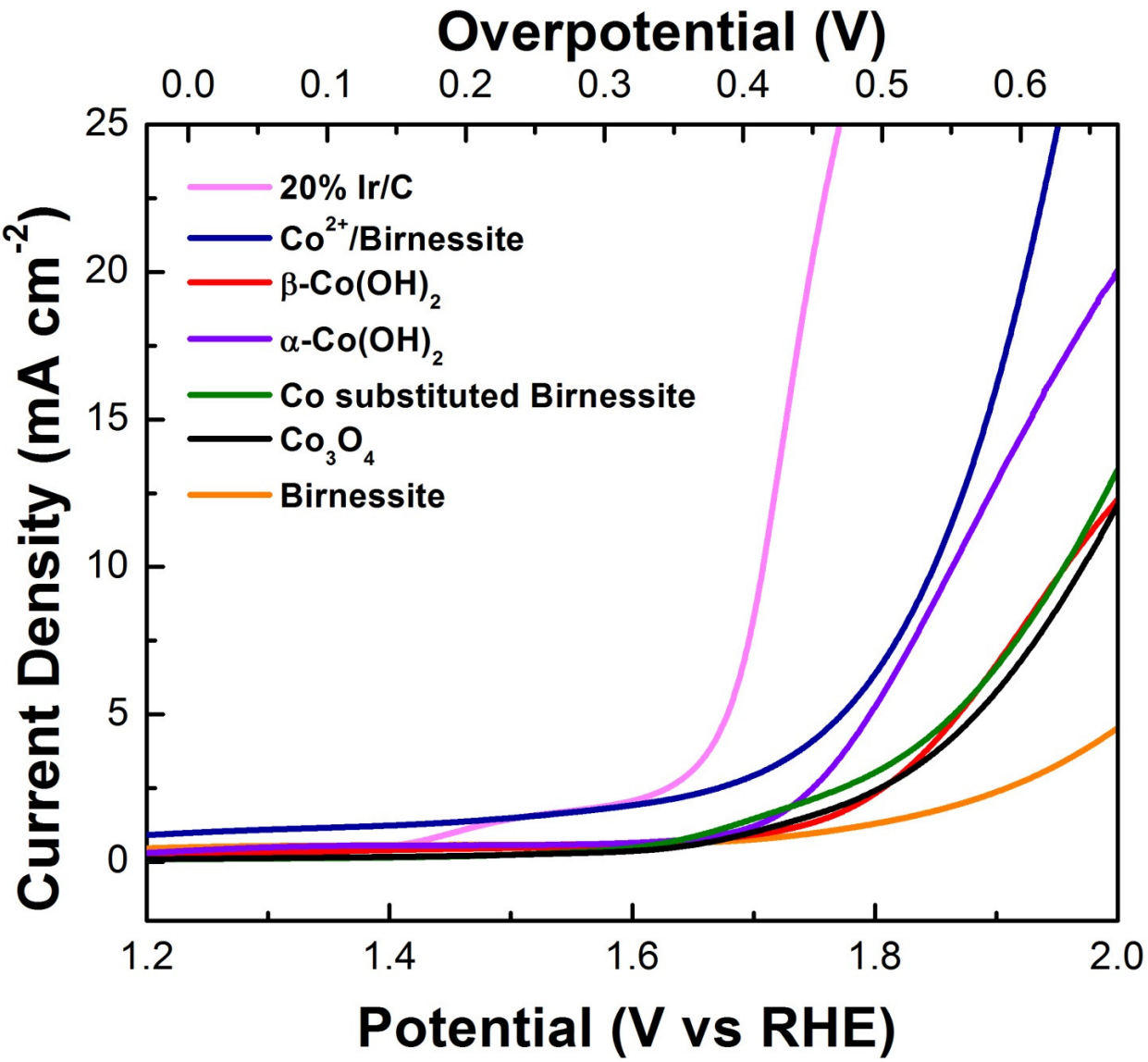

Figure S11. Polarization curves for Ir/C, Co^{2+}/birnessite, Co-substituted birnessite, birnessite, and cobalt hydroxides collected in phosphate buffer (pH 7).

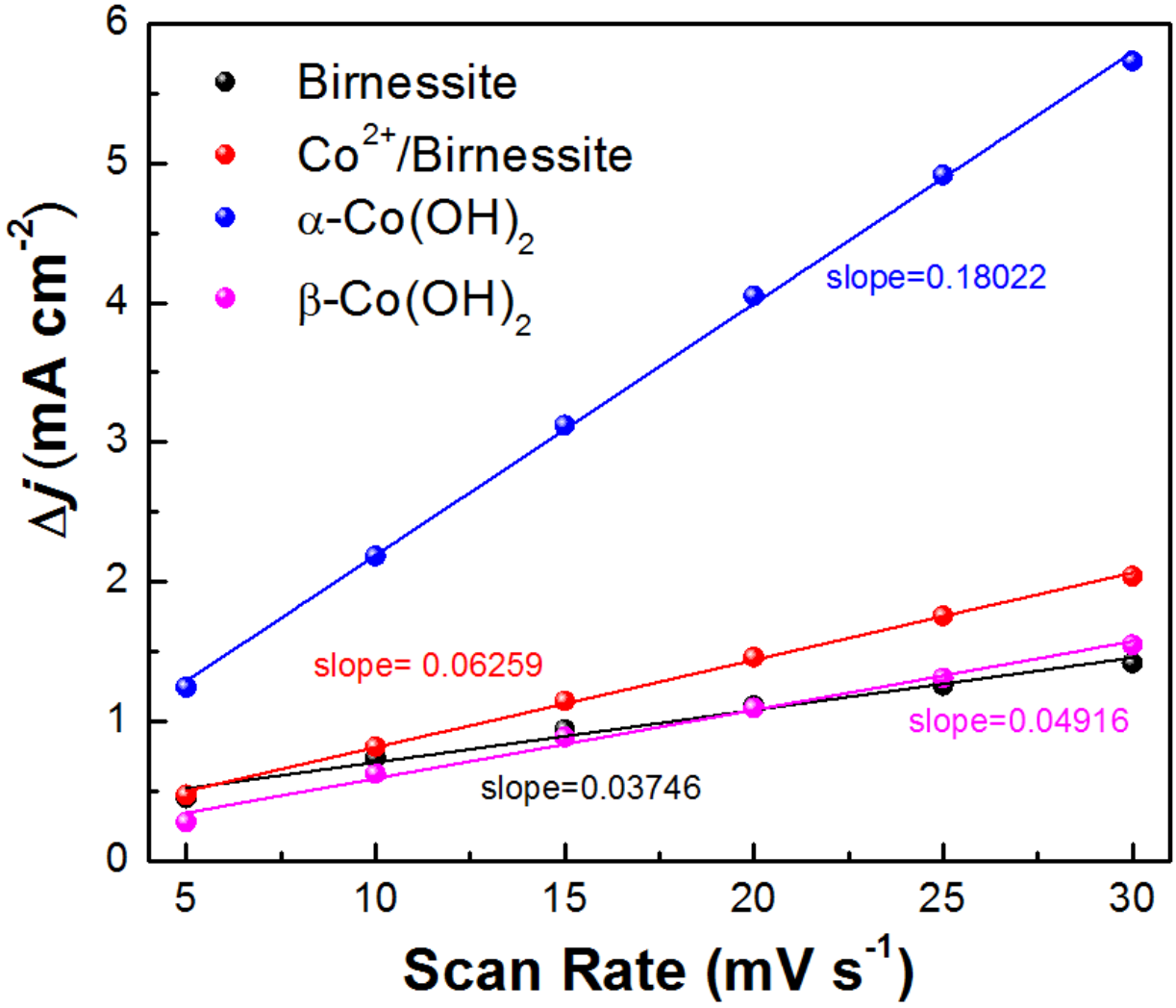

Figure S12. The difference in current density ($(\Delta j=j_a-j_c)$ at open circuit potential (OCP) plotted against scan rate fitted to a linear regression to estimate the ECSA of birnessite, Co^{2+}/Birnessite, α-$Co(OH)_2$ and β-$Co(OH)_2$.

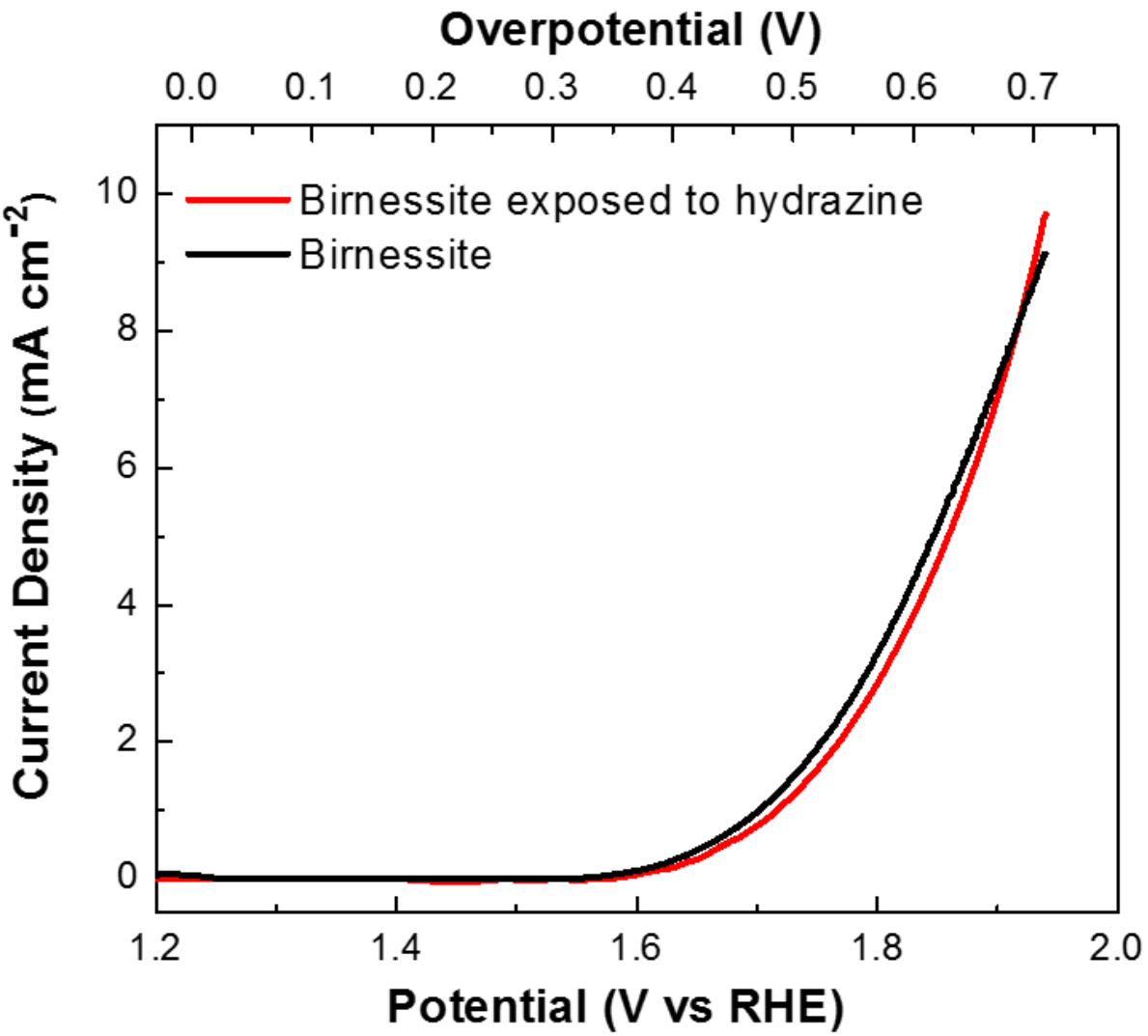

Figure S13. Polarization curves for birnessite and birnessite exposed to hydrazine in 1 M KOH. The results suggest that reaction with hydrazine does not improve the catalytic performance of birnessite.

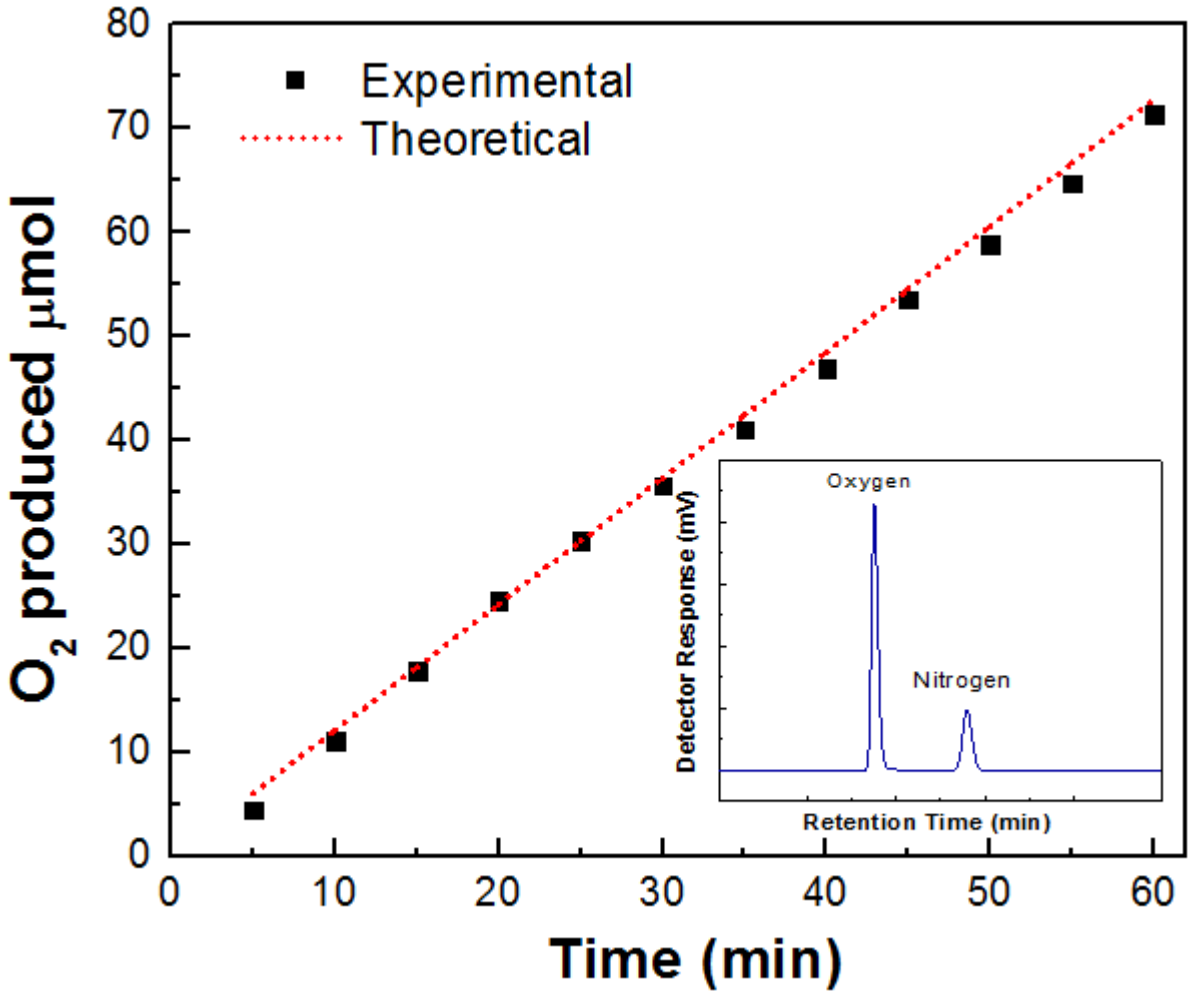

Figure S14. O_2 evolution from Co^{2+}/birnessite as a function of electrolysis time at a constant current of 7 mA. Inset shows an example of the detector response (from GC) for evolved oxygen.

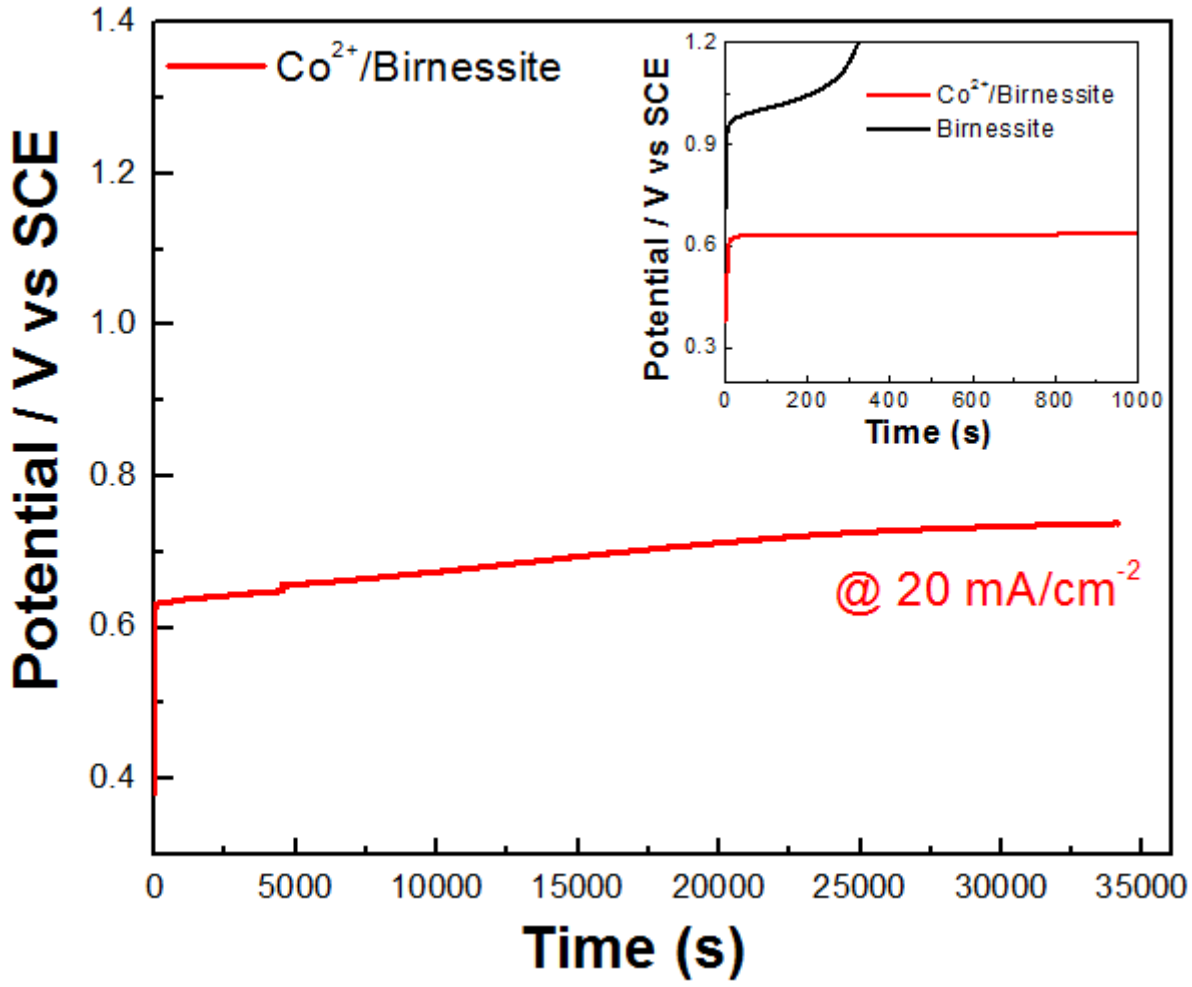

Figure S15. Chronopotentiometry curves for Co^{2+}/birnessite at a current density of 20 mA cm^{-2} using CFP as the working electrode. Inset is the chronopotentiometry of birnessite performed at 10 mA cm^{-2}.

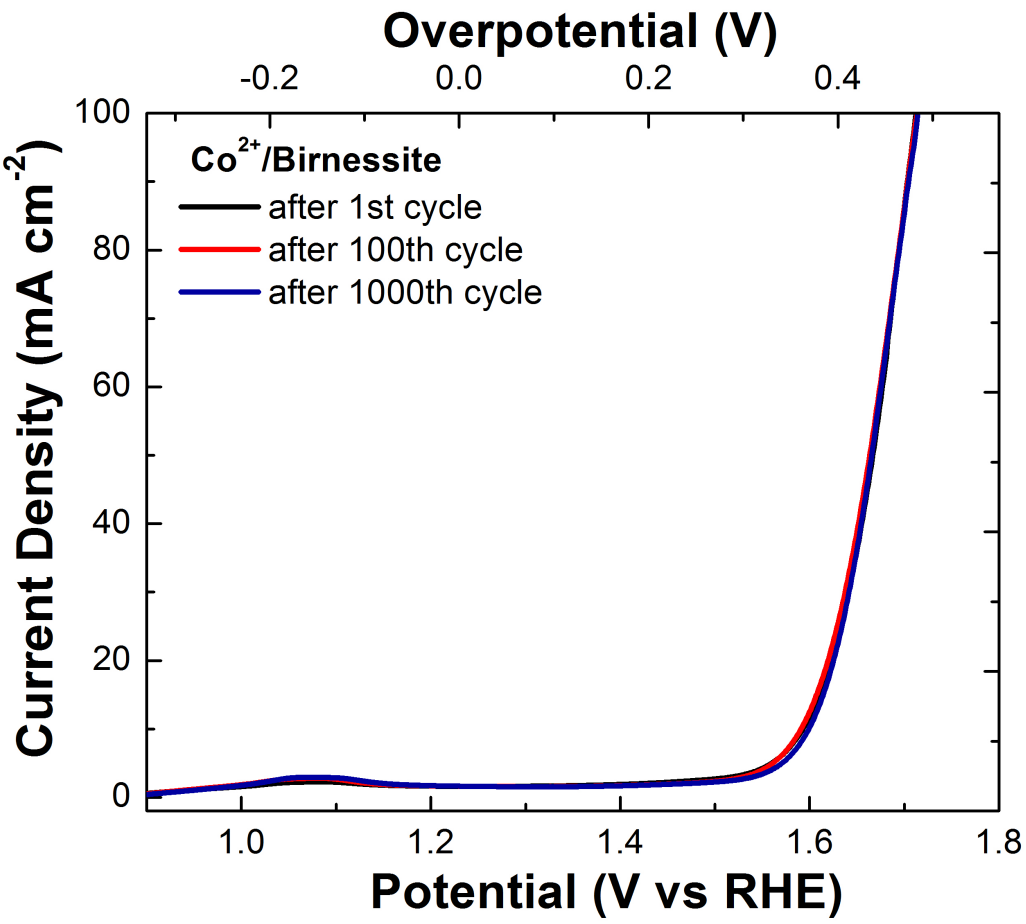

Figure S16. Polarization curves for Co^{2+}/birnessite with increasing electrochemical cycles.

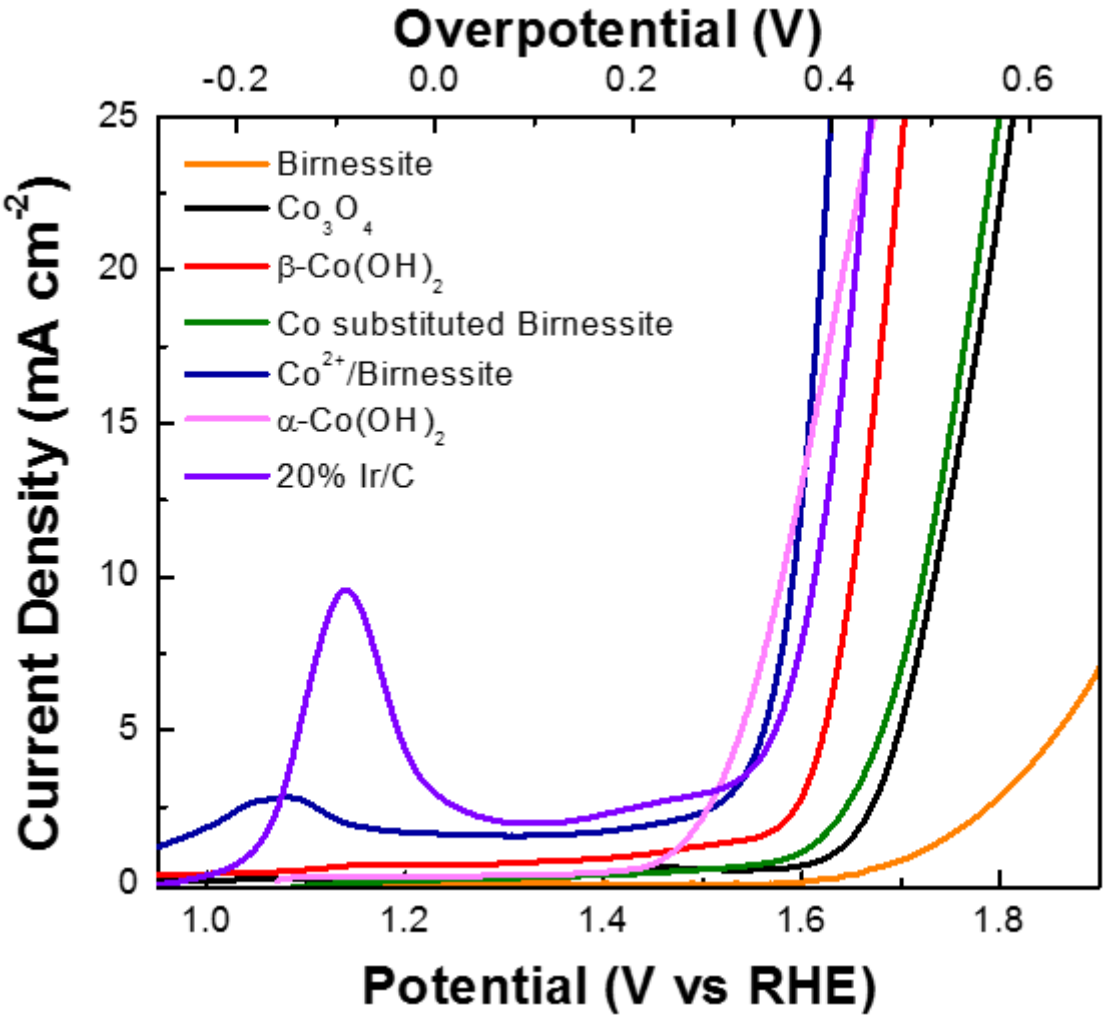

Figure S17. Polarization curves for Ir/C, Co^{2+}/birnessite, Co-substituted birnessite, birnessite, and cobalt hydroxides collected in 1 M KOH.

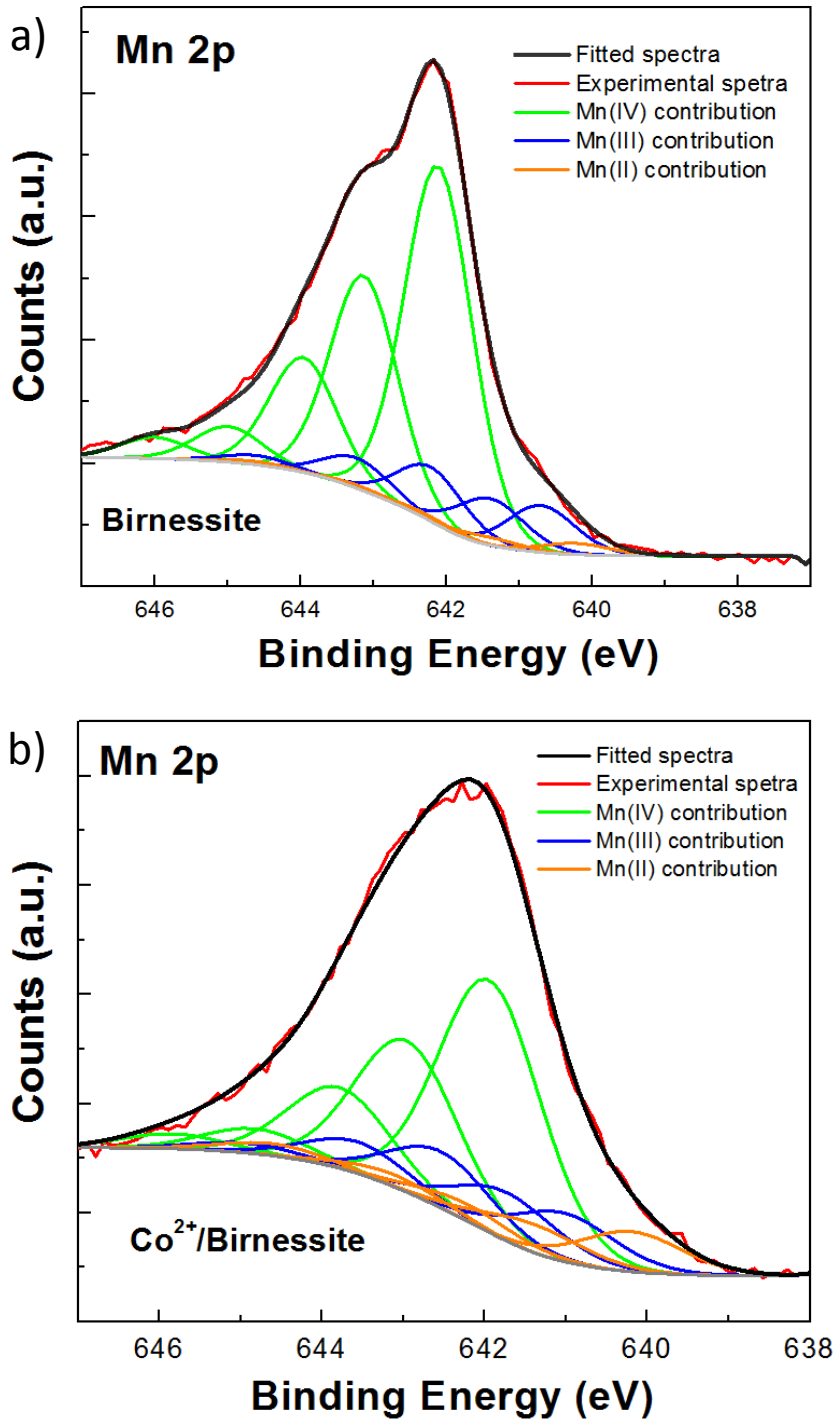

Figure S18. Mn $2p_{3/2}$ core level spectra of birnessite and Co^{2+}/birnessite. Mn(IV) fits are shown in green, Mn(III) fits are shown in blue and Mn(II) fits are shown in orange. The spectral fitting suggests that average oxidation state of Mn has decreased in from 3.74 to 3.57 after cobalt becomes intercalated in birnessite.

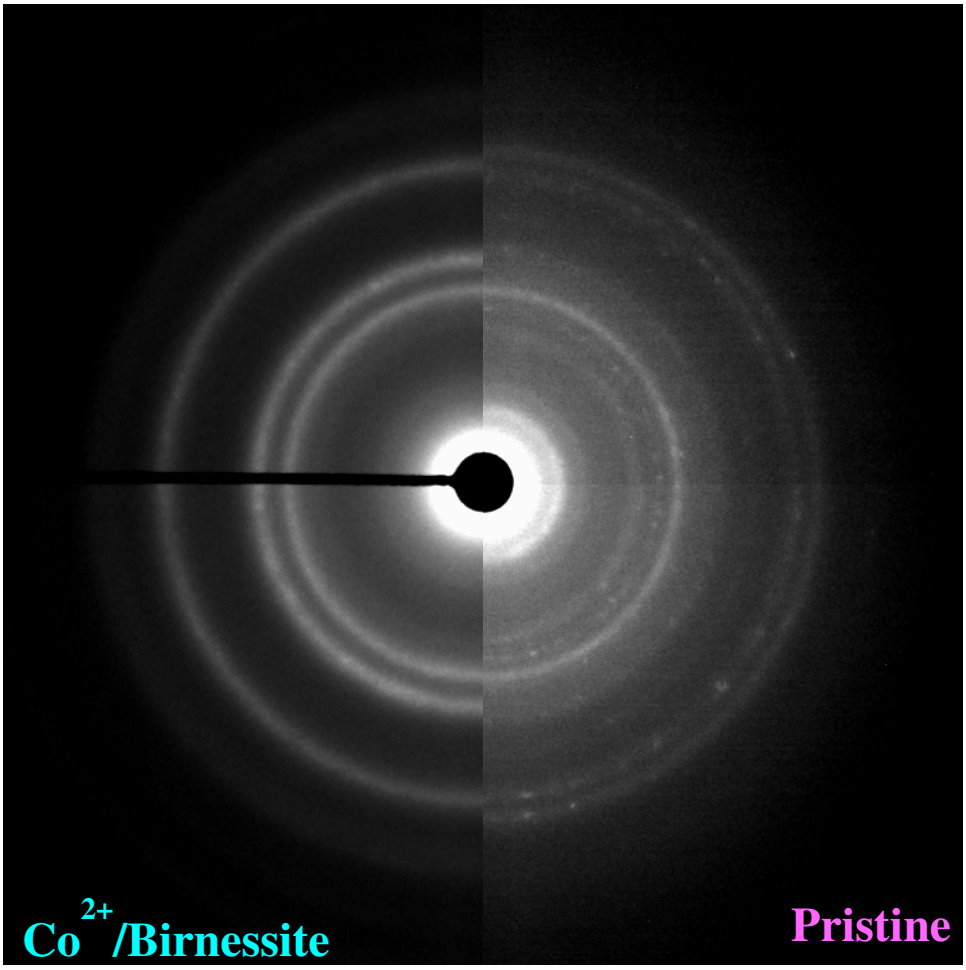

Figure S19. SAED patterns taken from Co-birnessite (left half) and pristine birnessite (right half) showing significant difference in crystallinity. Sharper rings and diffraction from more planes suggest better crystallinity in pristine birnessite.

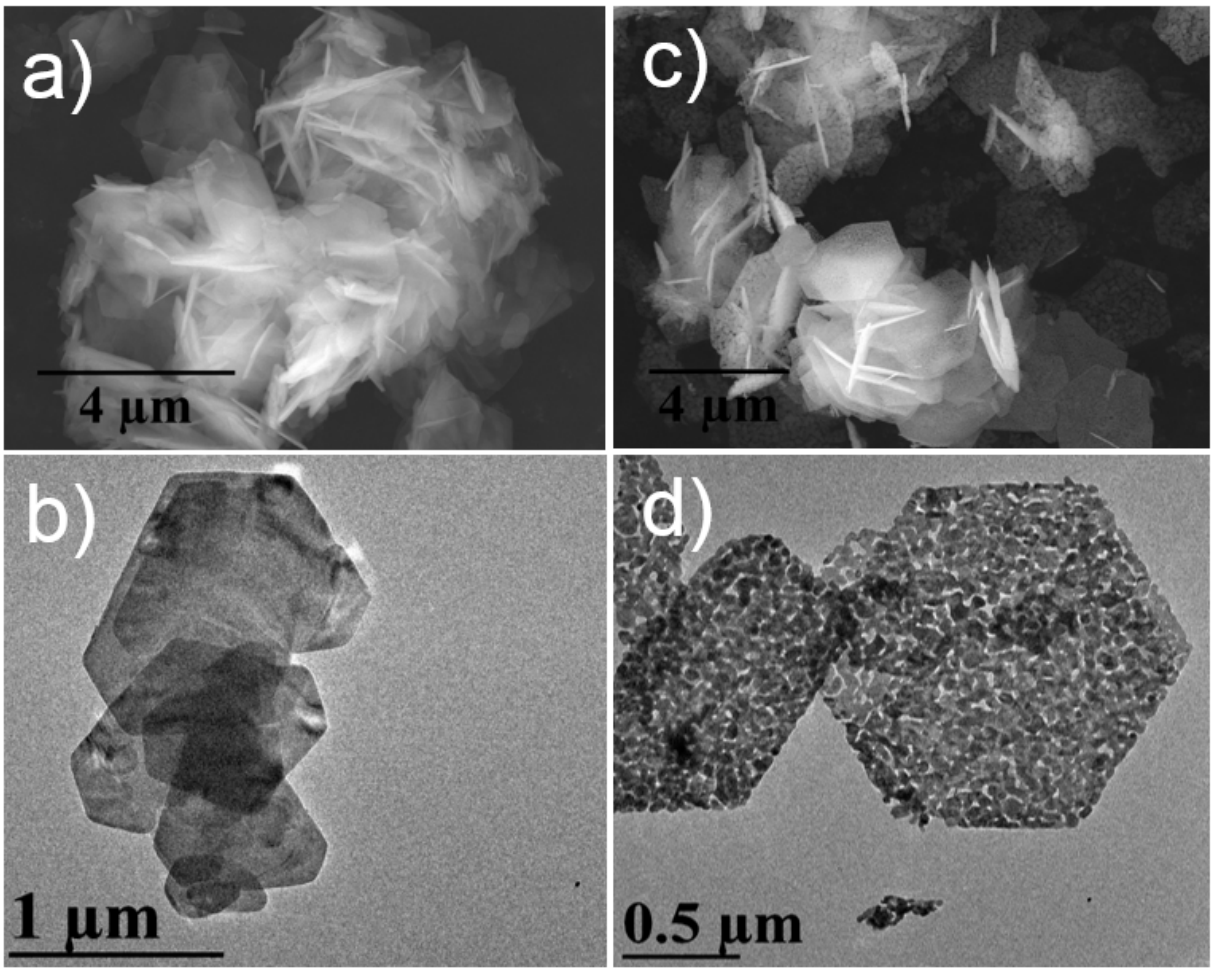

Figure S20. Electron micrographs of α-$Co(OH)_2$: (a) SEM and (b)TEM. Micrographs of Co_3O_4: (c) SEM and (d) TEM.

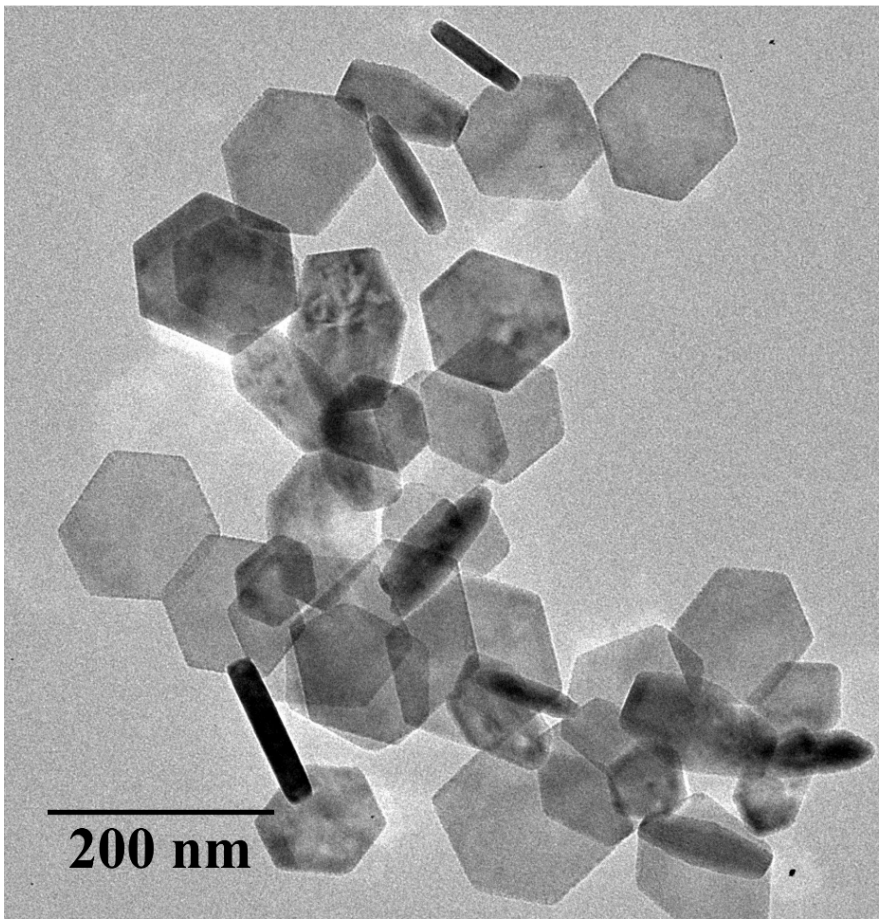

Figure S21. TEM micrograph of β-$Co(OH)_2$.

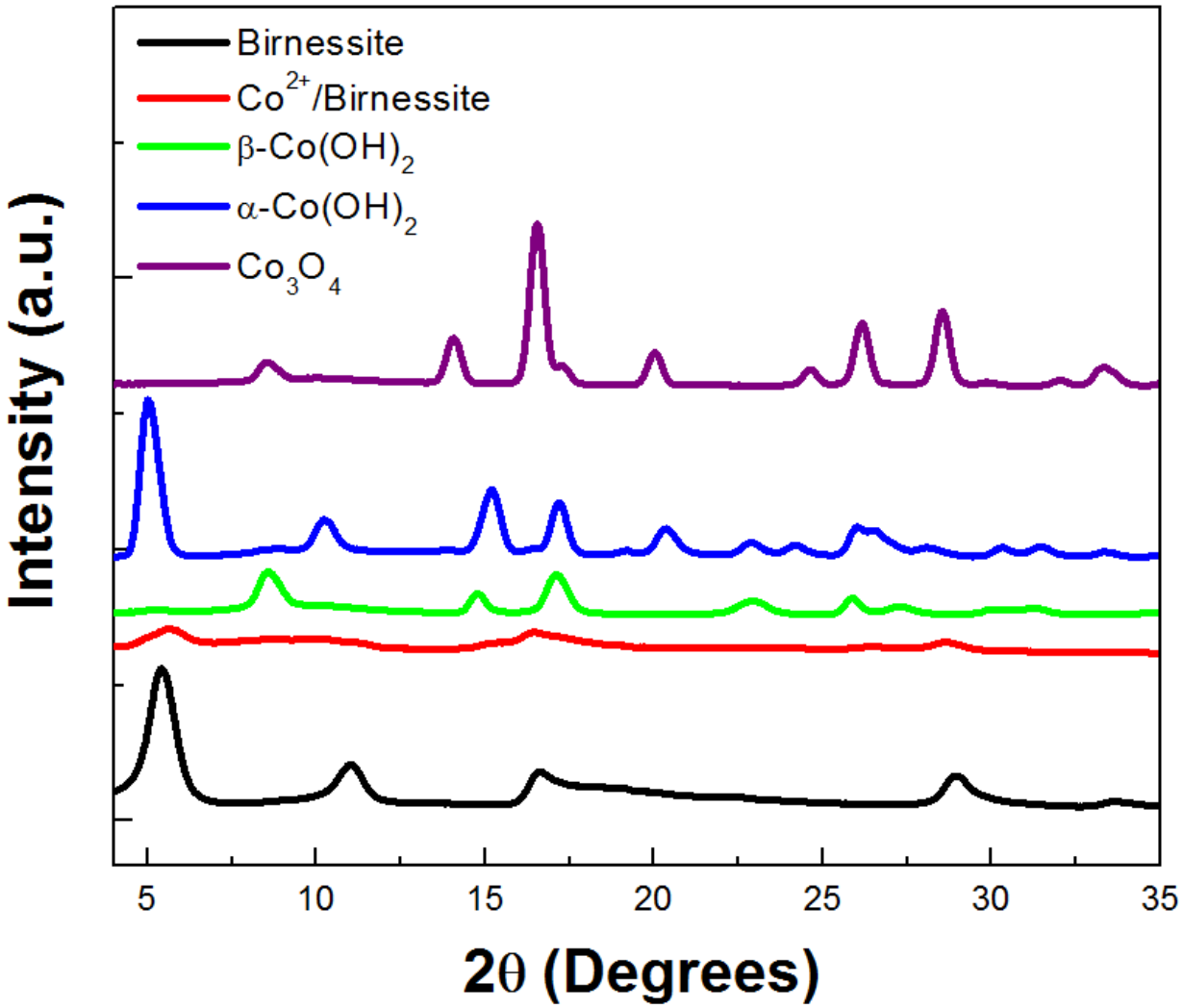

Figure S22. XRD spectra of α-$Co(OH)_2$, β-$Co(OH)_2$, Co_3O_4, birnessite, and Co^{2+}/birnessite.

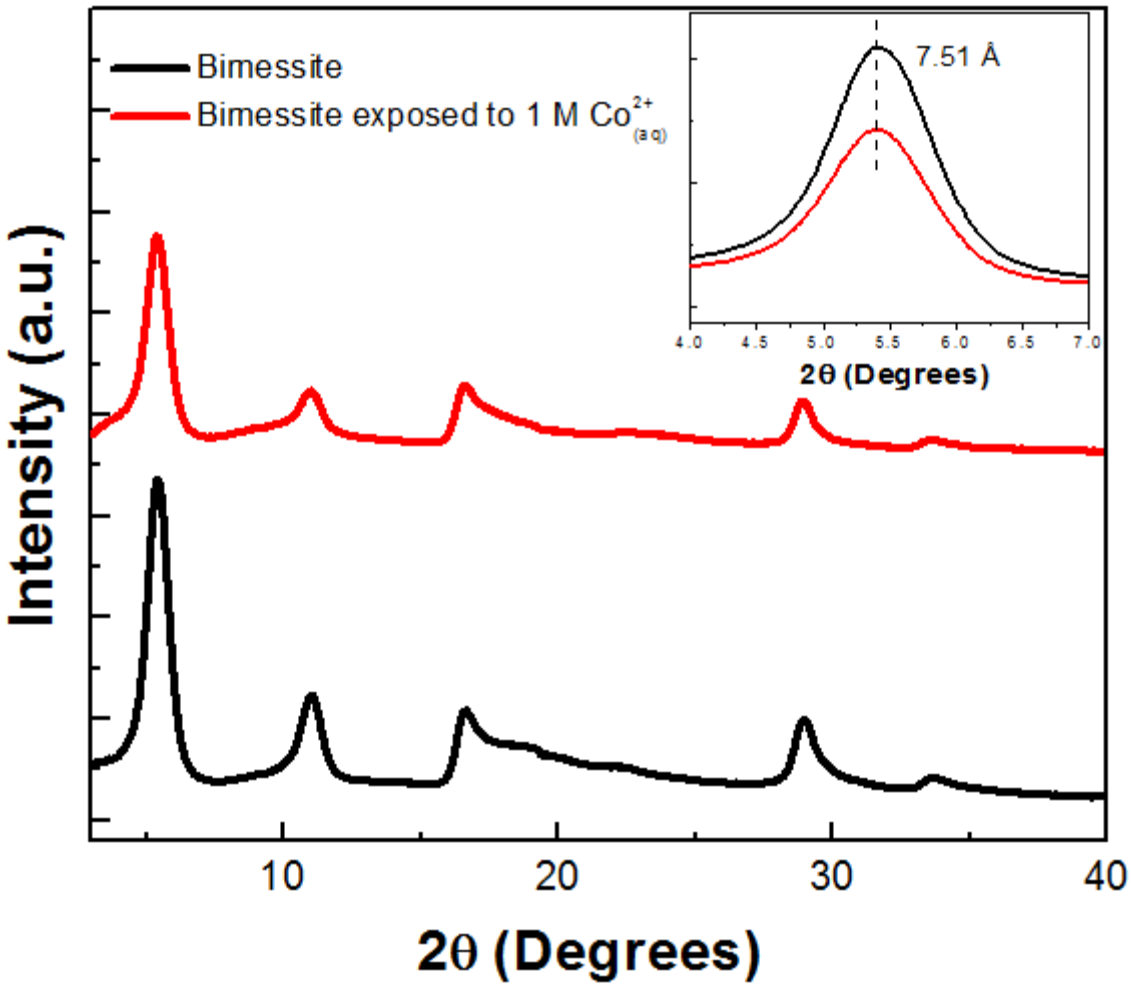

Figure S23. XRD diffractograms of birnessite and birnessite exposed to 1 M Co^{2+}. Inset is the enlarged (001) region that corresponds to the interlayer spacing. The inset suggests surface adsorbed cobalt does not alter the interlayer spacing.

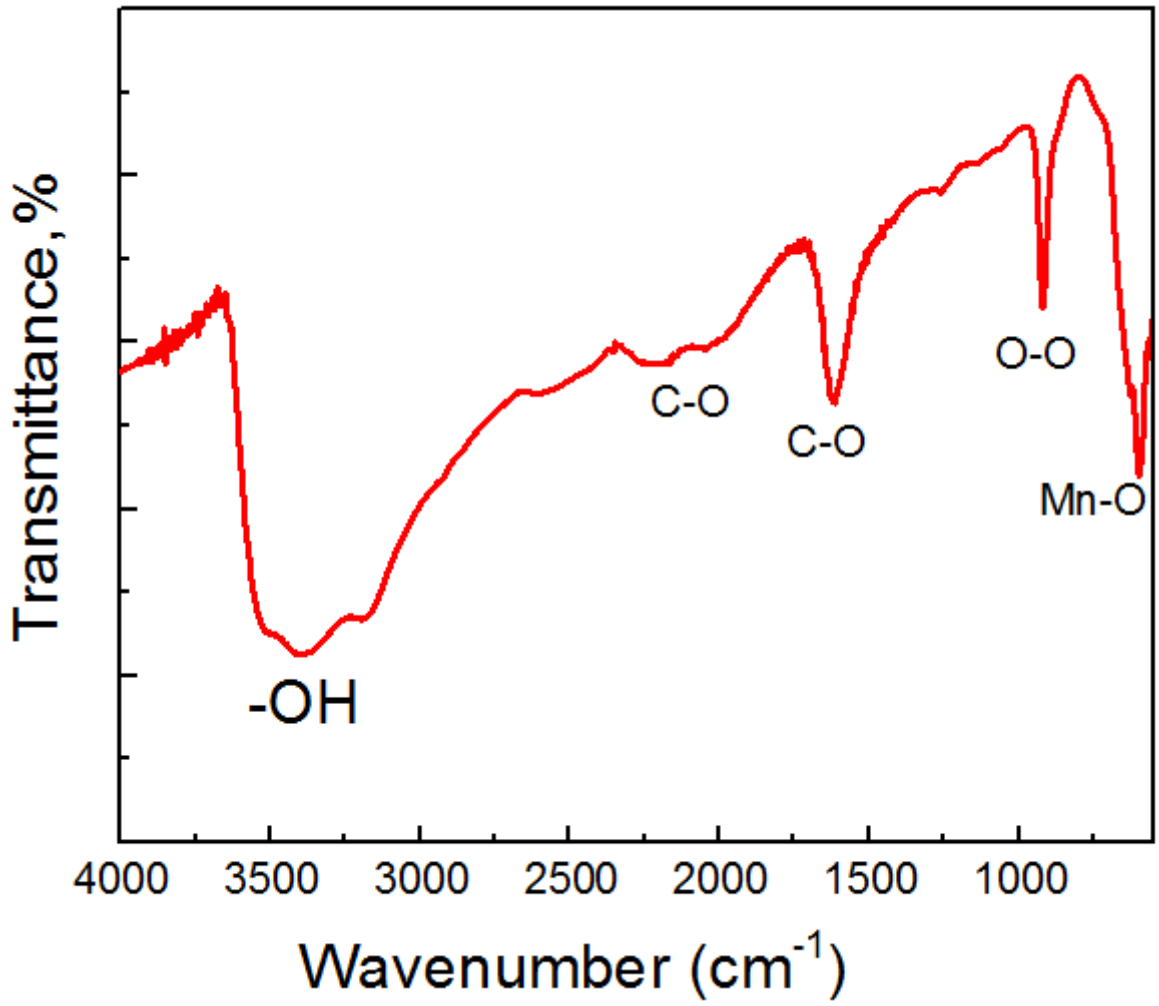

Figure S24. FTIR spectra of birnessite.

Table S1. Summary of OER activities in phosphate buffer.

Catalyst	**η (mV) at 10 mA cm^{-2}**	**TOF (s^{-1}) at η=0.50 V**	**mass activity (A g^{-1}) at η=0.50V**	**Tafel slope(mV dec^{-1})**
birnessite	920	0.0012	7	238±6
Co^{2+}/birnessite	618	0.0064	25	98±3
Co-substituted birnessite	725	0.0031	14	168±7
β-$Co(OH)_2$	725	0.0022	8.9	124±3
α-$Co(OH)_2$	632	0.0051	21	92±2
Co_3O_4	740	0.0057	8.9	173±4
20% Ir/C	480	0.23	100	60±3

Table S2. Experimental data for birnessite.

Sample	K:Mn	Co:Mn	Mn(IV)	Mn(III)	Mn(II)	AOS[a]	formula
Birnessite	0.31	-	75.8	22.3	1.9	3.74	$K_{0.31}MnO_{2.02}.0.54\ H_2O$
Co^{2+}/Birnessite	-	0.12	67.2	22.7	10.1	3.57	$Co_{0.12}MnO_{1.97}.1.56H_2O$
Co-substituted Birnessite	0.12	0.12	65.12	3.65	-	3.65	$K_{0.12}Co_{0.108}Mn_{0.9}O_2.0.48H_2O$

[a] AOS, average oxidation state of manganese were determined via XPS (Figure S15).
The K:Mn ratios determined by ICP-OES and EDS.
Formula was determined using the XPS,ICP-OES and EDS.